# Differential-Concentration Scanning Ion Conductance Microscopy

David Perry,[1, †] Ashley Page,[1,2, †] Baoping Chen,[1] Bruno G. Frenguelli[3] and Patrick R. Unwin[1,*]

[1]Department of Chemistry, [2]MOAC Doctoral Training Centre, [3]School of Life Sciences, University of Warwick, Coventry, CV4 7AL, United Kingdom.

† These authors contributed equally to this work

*corresponding author

p.r.unwin@warwick.ac.uk

+44 2476523264

**ABSTRACT**

Scanning ion conductance microscopy (SICM) is a nanopipette-based scanning probe microscopy technique that utilizes the ionic current flowing between an electrode inserted inside a nanopipette probe containing electrolyte solution, and a second electrode placed in a bulk electrolyte bath, to inform on a substrate of interest. For most applications to date, the composition and concentration of the electrolyte inside and outside the nanopipette is identical, but it is shown herein that it can be very beneficial to lift this restriction. In particular, an ionic concentration gradient at the end of the nanopipette, generates an ionic current with a greatly reduced electric field strength, with particular benefits for live cell imaging. This differential concentration mode of SICM (ΔC-SICM) also enhances surface charge measurements and provides a new way to carry out reaction mapping measurements at surfaces using the tip for simultaneous *delivery* and *sensing* of the reaction rate. Comprehensive finite element method (FEM) modeling has been undertaken to enhance understanding of SICM as an electrochemical cell, and to enable the interpretation and optimization of experiments. It is shown that electroosmotic flow (EOF) has much more influence on the nanopipette response in the ΔC-SICM configuration compared to standard SICM modes. The general model presented advances previous treatments, and provides a framework for quantitative SICM studies.

**KEYWORDS** Scanning ion conductance microscopy, electrochemical imaging, localized delivery, electroosmotic flow, finite element method.

## INTRODUCTION

Scanning ion conductance microscopy (SICM) is a powerful non-contact imaging technique capable of high-resolution topographical measurements.[1,2] In particular, SICM has found wide application in visualizing living cells,[3–6] at probe distances (separations) of tens of nanometers from the cell surface.[7,8] SICM experiments utilize a glass or quartz nanopipette filled with electrolyte solution as the scanning probe. A quasi-reference counter electrode (QRCE) is placed in the nanopipette probe and, typically, a bias is applied between the probe electrode and another electrode in bulk solution, that bathes a sample, to drive an ionic current through the end of the nanopipette between the 2 electrodes.[2] As the nanopipette approaches an interface, the ionic current often decreases as the gap resistance between the probe and surface increases.[2] Thus, the ionic current can be used as feedback to position the nanopipette near a substrate, and obtain topographical information by moving the nanopipette.[2]

Since its inception,[1] there have been several key developments in both the feedback types and scan regimes that can be used for SICM.[2,9,10] These include the introduction of modulated feedback types[11–13] and hopping scan regimes[5,14–16] which have improved both the stability and versatility of the technique. There has been a recent drive to develop SICM for multifunctional imaging,[10] begetting more complex scan regimes and probes to obtain a wealth of information on interfaces and interfacial processes. These capabilities include the detection of electrochemical reactions,[17,18] the surface charge of cellular membranes,[7,8,19,20] and quantitative monitoring of cellular uptake of electroactive molecules.[21] Several of these studies have demonstrated the importance of minimizing the applied bias in SICM experiments.[7,8,19] For example, it has been demonstrated that the larger the applied bias between the 2 electrodes, the greater is the convolution of topographical information with other surface properties, particularly surface charge, with important implications for the precision of SICM topographical measurements.[19,22]

The tip and bathing solutions usually have the same composition, but some SICM and nanopipette studies have used different electrolyte solutions in the nanopipette and the bulk solution.[21,23,24] There are several advantages of such conditions, including the local delivery of molecules for printing and patterning[24–27] or in studies of cellular uptake.[21] Hitherto, however, the effect of different electrolyte solutions on the potential distribution between the tip and bulk electrodes, and mass transport in SICM, has largely been ignored.

In this contribution, we analyze this differential concentration (ΔC)-SICM mode and demonstrate practically how it can be used to map topography and improve the sensitivity and versatility of functional measurements with SICM. In particular, ΔC-SICM can be used to probe cellular surface charge using a dilute electrolyte solution in the tip and physiological conditions in the bathing solution. The precision is better (wider dynamic range of the SICM current to surface charge) than previous SICM methods. Further, ΔC-SICM can be used with a higher electrolyte in the tip compared to the bathing solution, as a new approach to *image electrochemical reactions* at an electrode surface *purely via the SICM response*, as exemplified with a study of dopamine oxidation at a carbon fiber electrode.

The work herein develops a comprehensive understanding of the potential distribution and mass transport in ΔC-SICM, highlighting the importance of the liquid junction potential at the nanopipette end and electroosmotic flow (EOF), compared to conventional SICM. Significant outcomes of this work are that interfaces can be studied by SICM with minimal electric field effects and that topography and other physicochemical phenomena can be separated in a robust manner through the rational design of experiments.

## EXPERIMENTAL SECTION

### Solutions

Milli-Q reagent grade water (resistivity ca. 18.2 MΩ cm at 25°C) was used for all solutions. PC-12 cells were cultured and imaged in RPMI 1640 media containing 15% horse serum, 2.5% fetal calf serum, 5 mM glutamine, 100 U/mL penicillin and 100 μg/mL streptomycin (all Sigma Aldrich). The nanopipette tip, for topographical and surface charge measurements of living cells, contained a 100-fold dilution of the full cell culture media. This environment allowed the cells to function normally, as the composition of the solution at the cellular interface was largely maintained, with the local environment near the end of the nanopipette only transiently perturbed while making an SICM measurement. For reaction mapping experiments, a 10 mM KCl solution was used as the bulk electrolyte whilst the nanopipette contained either 80 mM KCl (for control experiments) or 50 mM KCl and 30 mM dopamine hydrochloride (unbuffered, pH 6.7).

**Nanopipettes and Electrodes**

Nanopipettes were pulled from borosilicate glass capillaries (o.d. 1.2 mm, i.d. 0.69 mm, Harvard Apparatus) using a laser puller (P-2000, Sutter Instruments; pulling parameters: Line 1: Heat 330, Fil 3, Vel 30, Del 220, Pul -; Line 2: Heat 330, Fil 3, Vel 40, Del 180, Pul 120). The inner radius of probes was measured using a JEOL 2000FX transmission electron microscope (TEM) to be 90 nm ± 5 nm. Two Ag/AgCl quasi-reference counter electrodes (QRCEs), one in the nanopipette and a second in bulk solution, were used for both topographical and charge mapping. These were AgCl-coated wires prepared as described previously.[28] For reaction mapping experiments, a carbon fiber (CF) was used as a substrate working electrode and was electrically connected to allow a potential offset to be applied with respect to the bulk QRCE (see 'Substrate Preparation'). The potential of the Ag/AgCl wires in each of the above solutions measured vs. a saturated calomel electrode (SCE) were determined as in Supporting Information, Section (SI-)1, Table S1, to yield the potential of the nanopipette electrode with respect to the electrode in bulk, $\Delta E_{Electrode}$. With this knowledge, it was also

possible to estimate the liquid junction potential, $E_{junction}$, at the end of the nanopipette, for a given set up, as reported in SI, Table S2.

**Cell Culturing Procedure**

Adherent PC-12 cells (ATCC-CRL-1721.1) were cultured in tissue culture flasks in the above-specified media until confluent, before trypsinization and transfer to Petri dishes. They were allowed 72 hours to adhere to the glass substrate before imaging in fresh media.

**Substrate Preparation**

The PC-12 cells used were adherent to glass-bottomed petri dishes (3512, WillcoWells) and these were used as a support. Individual CFs (diameter 7 μm) were adhered to a glass microscope slide using a piece of Kapton tape to mask most of the carbon fiber. The bias applied to the carbon fiber was *via* copper wire connected to one end of the fiber with conductive silver paint.

**Instrumentation**

The lateral movement of the sample was controlled using a two-axis piezoelectric positioning system with a range of 300 μm (Nano-BioS300, Mad City Labs, Inc.), while movement of the nanopipette probe normal to the substrate was controlled using a piezoelectric positioning stage of range 38 μm (P-753-3CD, Physik Instrumente), to which the probe was mounted. The current-voltage converter used was made in-house, while user control of probe position, voltage output and data collection was *via* custom made programs in LabVIEW (2013, National Instruments) through an FPGA card (7852R, National Instruments).

**ΔC-SICM Mapping**

For approach curve measurements, the nanopipette was approached towards the glass substrate (*z* direction) at a speed of 2 μm/s (with the position of the probe in the *x*-*y* plane of the substrate fixed). Topographical scans were performed in a scan hopping regime that generated pixel-by-pixel maps, with full details and example topographical maps shown in SI-2, Figure S1. FEM

simulations, which demonstrate the insensitivity to surface charge under topographical mapping conditions, are shown in Figure S2.

All functional measurements were made in a scan hopping regime. A full description of the surface charge mapping experimental protocol can be found in SI-3 (Figure S3) along with the data normalization procedure. Full details of the reaction mapping experimental protocol can be found in SI-4, along with a schematic (Figure S4), and bulk substrate voltammetry (Figure S5).

**FEM Simulations**

A 2D axisymmetric cylindrical model of the nanopipette at different distances from a substrate was constructed in COMSOL Multiphysics (version 5.2a) with the Transport of Diluted Species, Laminar Flow and Electrostatics modules. Full simulation details, including a schematic of the simulation domain and boundary conditions are presented in SI-5 (Figure S6). The dimensions of the nanopipettes used experimentally were determined from TEM images to ensure that simulations faithfully modeled experiments.

## RESULTS AND DISCUSSION

### General Considerations

In ΔC-SICM, there is a potential difference between the two Ag/AgCl QRCEs because of the different solution environments:

$$\Delta E_{Electrode} = E_{Electrode,tip} - E_{Electrode,bulk} \quad (1)$$

in which $E_{Electrode,tip}$ is the potential of the QRCE in the environment pertinent to the inside of the nanopipette, and $E_{Electrode,bulk}$ is the potential of the QRCE in the bathing solution (values in SI-1, Table S1). The difference in concentration internally and externally, near the end of the nanopipette, also gives rise to a junction, or diffusion potential. Further, an external

potential, $E_{external}$, can be applied across the two electrodes. Thus, the total potential between the 2 electrodes in the ΔC-SICM configuration (Figure 1) is:

$$E_{total} = \Delta E_{Electrode} + E_{junction} + E_{external} \quad (2)$$

ΔC-SICM can be used flexibly, with the higher concentration electrolyte solution in the probe or the bulk solution (*vide infra*). For each experimental configuration used, the values of $\Delta E_{Electrode}$ and $E_{junction}$ are stated in SI-1, Table S2.

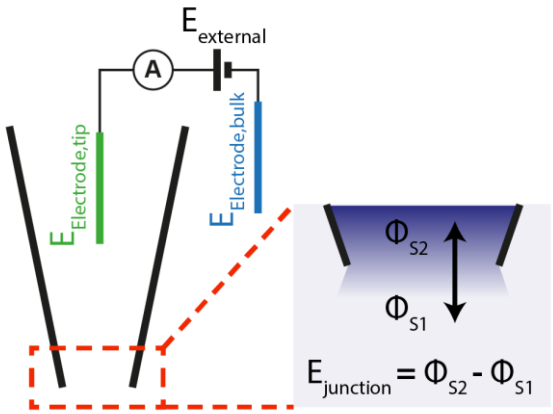


**Figure 1.** Schematic of the potential differences in ΔC-SICM. A difference in electrolyte concentration (composition) inside and outside the nanopipette leads to different equilibrium potentials, $E_{Electrode,tip}$ and $E_{Electrode,bulk}$, of the two QRCEs and a diffuse junction potential, $E_{junction}$, at the end of the nanopipette where the two solutions of potential $\phi_{S2}$ (in the tip) and $\phi_{S1}$ (in the bathing solution) meet. An external bias, $E_{external}$, may also be applied.

FEM simulations allowed the electric field at the end of the nanopipette to be readily calculated. It is informative to compare the case for ΔC-SICM live cell imaging herein, where $E_{external} = -\Delta E_{Electrode}$, so that $E_{total} \approx E_{junction}$ to conventional SICM imaging parameters e.g. a 100 mV tip bias, within the normal range of values applied,[3–5,14,15,20,29] and the same concentration (physiological conditions) in the bath and tip. These cases are presented

and compared in Figure 2, with the tip in bulk solution. Under the conventional SICM conditions (a), an electric field of up to 40 kV/m is established at the end of the nanopipette. It can be seen that with only the liquid junction potential (b), the only significant electric field arises from the double layer due to the negative charge on the walls of the charged nanopipette ($\sigma_{tip}$=-30 mC/m$^2$, considered as typical for these conditions[30]). In the region at the nanopipette opening, the electric field is at least two orders of magnitude less than when a bias of 100 mV is applied between the inside and outside of the nanopipette, with the effect of $E_{junction}$ spread over a long distance (Figure 2c). In cases where the applied SICM bias is greater than 100 mV, the electric field strength would be significantly greater. Consequently, for delicate substrates such as living cells, which can be perturbed/stimulated by the presence of an electric field,[31–33] ΔC-SICM will be much less perturbing and less invasive. Example topographical maps of PC12 cells using ΔC-SICM with an approach bias of $E_{total} = E_{junction}$ are shown in SI-2, Figure S1, together with a simulated and experimental approach curve, which match well.

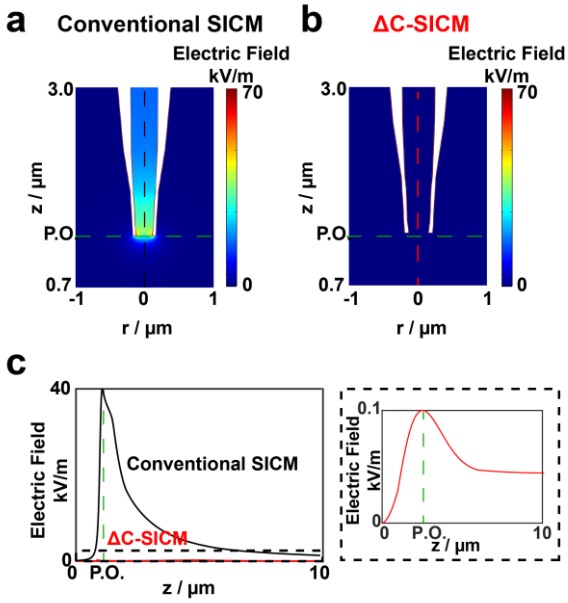


**Figure 2. a**) Electric field magnitude at the end of a 90 nm radius nanopipette in conventional SICM, with a 100 mV bias applied to the bulk electrode and the same electrolyte (103 mM

NaCl, 24 mM $NaHCO_3$ and 5 mM KCl) throughout. **b**) Electric field magnitude at the end of a 90 nm radius nanopipette under ΔC-SICM conditions ($E_{total} = E_{junction}$ and the same bath solution as for (a) but with a 100-fold dilution in the tip). c) Line profiles of the electric field strength in the *z*-direction at the axis of symmetry of the pipette with the peak (highlighted by the vertical green dashed line marked P.O.) corresponding to the nanopipette opening. Profile for typical SICM shown in black and ΔC-SICM in red, with the inset showing a zoom of the ΔC-SICM profile.

The different ionic conductivity between the inside and outside of the nanopipette in ΔC-SICM influences the shape of approach curves. For the surface charge and reaction mapping experiments that are discussed in the following sections, simulated approach curves for sensing the surface are shown in SI-5, Figure S7. Where a lower electrolyte concentration is present in the bulk solution compared to the nanopipette (as used for charge mapping of cells), the gap resistance accounts for a higher proportion of the total resistance, and a much shallower approach curve of ionic current *vs.* distance is seen, with the ionic current sensitive to the substrate from much greater distances. Where the concentration difference is reversed (as for reaction mapping/delivery), a sharper approach curve is seen, as the nanopipette resistance dominates, and the gap needs to be very small to have any influence on the current.

**Surface Charge Mapping with ΔC-SICM**

We have previously shown that it is possible to use SICM to map charge heterogeneities in cell membranes under physiological conditions (high ionic strength) even though the electrical double layer is compressed to a high degree.[20,22] Our approach is to use a self-referencing pulsed potential program, in which the nanopipette current response is measured near the surface and in bulk solution at each and every pixel, so that subtle differences in the nanopipette

electrochemical response can be determined.[8] Although under physiological conditions (ionic strength ~130 mM), the Debye length is less than 1 nm, the diffuse layer extends beyond this.[34] Most importantly, when the SICM tip is stationed beyond this nominal distance, e.g. herein at an approximate separation of 20 nm or more, the double layer at the substrate is perturbed (and sensed) by the electric field (and current) from the nanopipette orifice (*vide infra*). It is for precisely this reason that we have advocated the use of either bias modulation[19] (with zero net bias) or a small DC current[8] in conventional SICM to minimize perturbation of the double layer and obtain more faithful topographical information. In the same vain, as shown in SI-2, Figure S2, the nanopipette current response of ΔC-SICM with a small bias, such as $E_{total} = E_{junction}$, as used in Figure S1, is relatively insensitive to surface charge and can be used for quantitative topographical mapping.

In order to assess the application of ΔC-SICM for charge mapping, FEM simulations were performed with a nanopipette both in bulk solution and near a charged interface (27 nm separation, within the typical range of approach distances achieved). As part of these simulations, we also assess the importance of EOF in the SICM response. Previous studies have considered EOF to not significantly influence the response of nanopipettes and the SICM response, under a range of conditions,[22,35,36] and it can be advantageous to ignore due to computational expense.

The data in Figure 3 compare the normalized current response of typical conventional SICM to ΔC-SICM ($E_{total} = E_{junction}$), with and without EOF, for a range of negative surface charges (as typically predominant on cell membranes[7]); see SI-3 for experimental protocol and current normalization procedure. Note that as well as the solution compositions being different for the two techniques, the approach bias is different, but the applied potential for surface charge sensing in both cases is -0.4V applied to the nanopipette electrode. It is immediately apparent that EOF is an important consideration for ΔC-SICM and cannot be ignored. In the

case of conventional SICM, at the lower surface charge densities applied to the substrate, EOF has very little effect on calculated ionic currents, in line with previously reported studies.[10,22,35] However, as the surface charge increases beyond about -30 mC/m$^2$, EOF can be seen to be an important consideration.

It can be seen from Figure 3, that ΔC-SICM is more sensitive to surface charge (wider dynamic range of normalized current to surface charge) than conventional SICM, over a range of 80 mC/m$^2$ (considering EOF, full model). Thechanges in the normalized current signal with surface charge in Figure 3 may appear small, but are easily detected because of the pixel-level self-referencing implemented in the hopping mode protocol, as shown practically below.

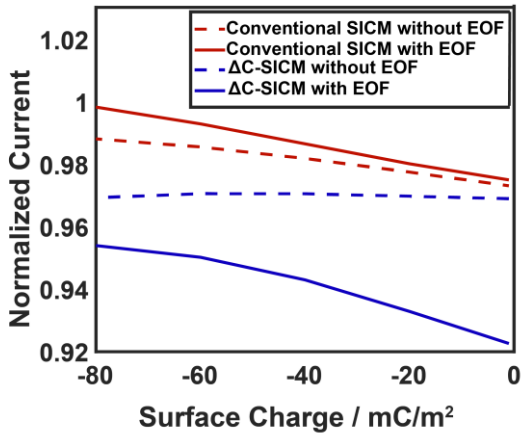


**Figure 3.** Normalized nanopipette current versus substrate surface charge density for a nanopipette with identical geometric (90 nm radius) and glass surface charge (-30 mC/m$^2$) for different modes and mass transport situations in SICM. Normalized currents were calculated 20 ms into a current-time (*I-t*) curve after applying an external bias of -400 mV to the nanopipette QRCE, jumped from the approach bias ($E_{external}$=$-\Delta E_{Electrode}$ in the case of ΔC-SICM, and from 100 mV for conventional SICM). The red lines are for conventional SICM (103 mM NaCl, 24 mM $NaHCO_3$ and 5 mM KCl in both the nanopipette and bath) and the blue lines are for ΔC-SICM (100-fold dilution of the bath solution present in the nanopipette). The dashed lines are simulations solving only the Nernst-Planck and Poisson equations, while the

solid lines also included EOF. The raw simulated ionic currents underlying these data are shown in SI-6, Figure S8.

Differences between ΔC-SICM (Figure 4a) and conventional SICM (Figure 4b), in terms of concentration profiles, electric field strength, and velocity profiles (from EOF) at the end of a nanopipette, near the most extreme negatively charged substrate (-80 mC/m$^2$), 20 ms after applying a bias of – 400 mV to the nanopipette electrode, are evident from in Figure 4. These data further highlight how it is possible to sense the double layer, with conventional SICM, at large distances from the interface, compared to the double layer dimension, because the double layer at the interface becomes perturbed by the applied electric field from the tip (Figure 4b(i)).

For ΔC-SICM, the double layer region is not perturbed in the same way (Figure 4a(i)) due to the greatly diminished electric field at the end of the nanopipette (Figure 4a(ii)). This diminished electric field can be explained by considering the electrolyte concentrations present in the nanopipette and bulk domains. In ΔC-SICM, where a lower electrolyte concentration is present in the nanopipette domain, the end of the nanopipette becomes more concentrated as solution from the bath moves into the nanopipette. Consequently, the region at the end of the nanopipette becomes less resistive, and the region of maximum electric field strength moves up into the nanopipette where the ionic strength is still low. However, ΔC-SICM is sensitive to surface charge, and the sensitivity is due to EOF.

Figure 4a(iii) shows a fluid velocity profile in ΔC-SICM with $E_{external} = -0.4$ V. It can be seen that between the charged nanopipette wall and the substrate there is a significant radial velocity bringing solution from outside the nanopipette into the narrow gap and up into the nanopipette domain. Under ΔC-SICM conditions, this movement of fluid is from an area of higher concentration (external to the nanopipette) to lower (in the nanopipette), greatly changing the ionic composition in the lower region of the nanopipette. For conventional SICM

(Figure 4b(iii)), EOF brings solution between two regions of similar concentration. Thus, although the fluid velocity tends to be higher in conventional SICM, compared to ΔC-SICM, (compare Fig 5a(iii) and Figure 4b(iii)), due to the higher electric field in the case of conventional SICM, the overall effect on mass transport, compared to ion migration is less. The velocity profiles also give an indication as to the resolution of ΔC-SICM for surface charge mapping. It can be seen that the region of greatest velocity, driven by surface charge and EOF, is between the walls of the pipette and the substrate, with the velocity dropping off to bulk by around 3/2 times the pipette diameter. This is similar to conventional SICM.[28] Future work could consider optimizing the nanopipette geometry, including the wall/lumen ratio, for enhancing surface charge sensitivity and resolution.

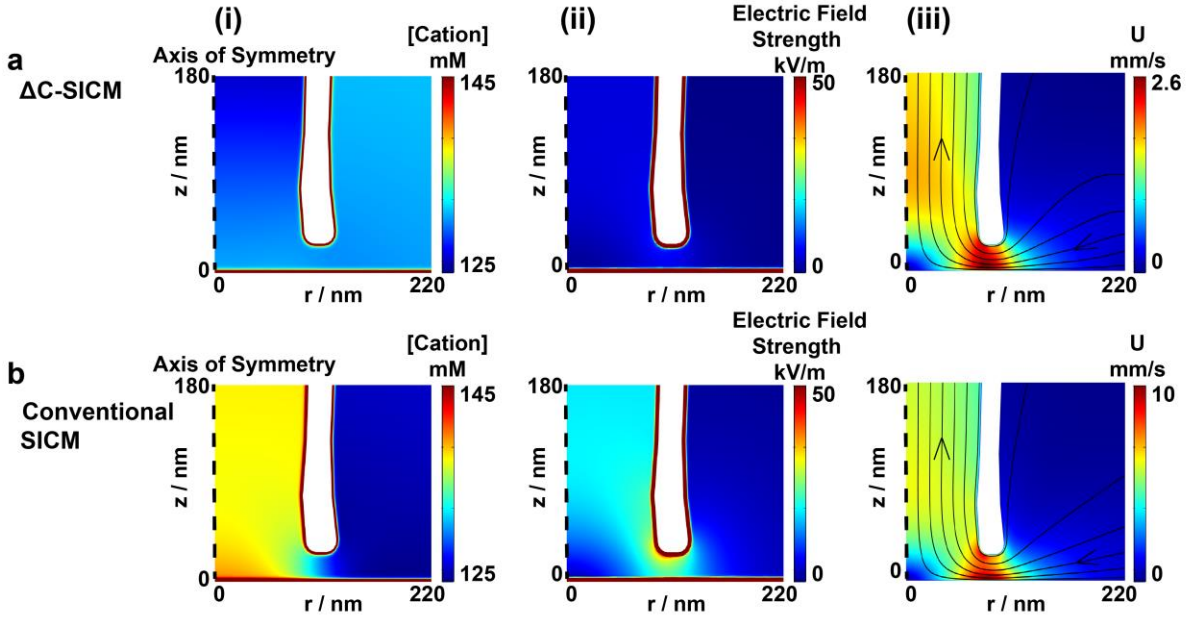


**Figure 4.** Cation concentration (i), Electric field strength (ii), and velocity profiles (iii) at the end of the nanopipette near a substrate with surface charge -80 mC/m$^2$ shown for: (a) ΔC-SICM with a 100-fold dilution in the nanopipette domain; and (b) conventional SICM with identical (physiological) concentrations in the nanopipette and bulk. All profiles are taken at $t$ = 20 ms after jumping the potential of the nanopipette electrode to -400 mV from either $E_{external} = -\Delta E_{Electrode}$, for ΔC-SICM (**a**), or from +100 mV for conventional SICM (**b**).

**ΔC-SICM Surface Charge Mapping**

ΔC-SICM measurements of surface charge and topography considered PC12 cells as the substrate. To minimize convolution between topography and other surface properties, an external bias, $E_{external}$, of 109 mV was applied to counter $\Delta E_{Electrode}$, so that $E_{total} \approx E_{junction}$ (≈20 mV) was used for topographical imaging.

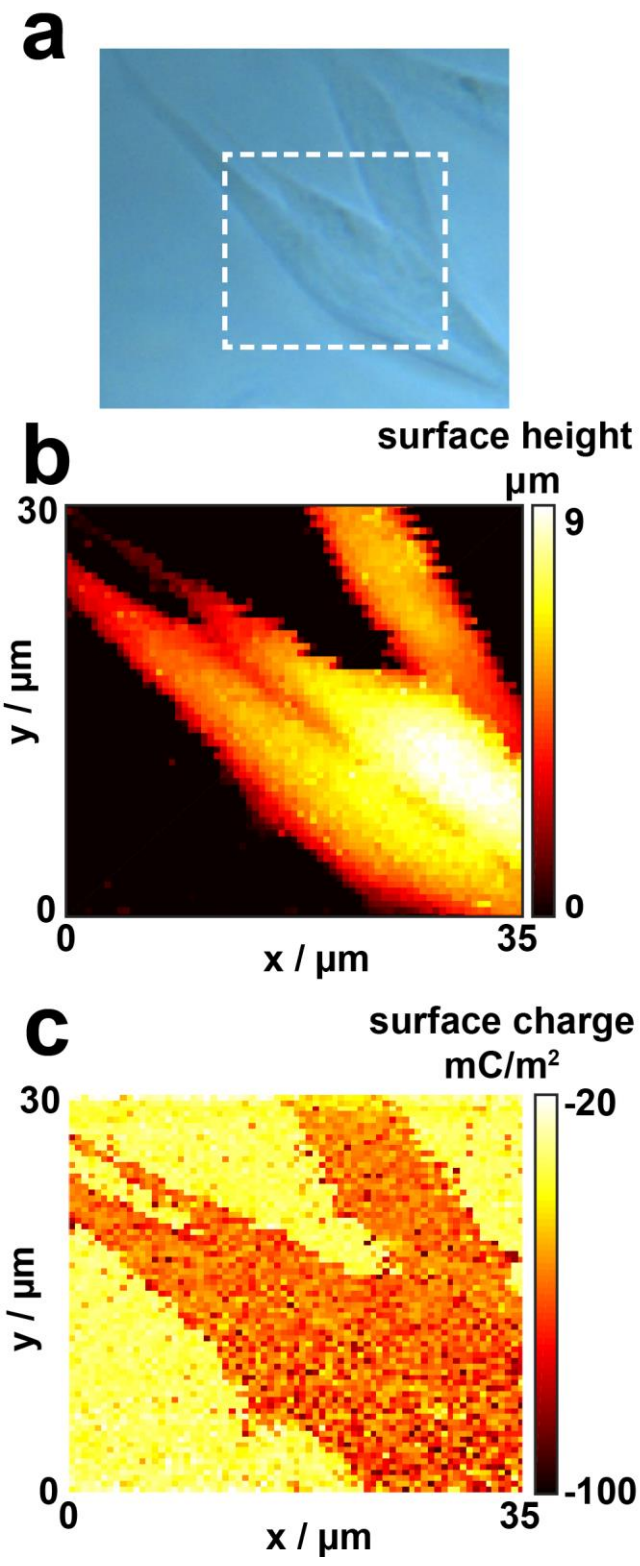


**Figure 5.** Topography and surface charge mapping of PC12 cells using ΔC-SICM. **a**) Optical micrograph of PC12 cells on a glass substrate, with the SICM scan area denoted by the white dashed rectangle. **b**) Topographical map collected with a ~90 nm radius nanopipette using ΔC-SICM and a driving potential of $E_{total} \approx E_{junction}$. A decrease of 5% in the ionic current

between the tip in bulk and near the surface was used as the set point, corresponding to a distance of 22 nm. **c**) Corresponding surface charge map (see SI-3 for normalization procedure) using a FEM-simulated calibration curve. Normalized current maps underpinning these data and the calibration curve are shown in SI-7, Figure S9.

Figure 5a shows an optical micrograph of a cluster of differentiated PC12 cells. The area denoted by the white dashed rectangle indicates the SICM scan area mapped with the pulsed potential regime described above. $E_{total} \approx E_{junction}$ was used to map the topography of the cellular surface (Figure 5b). For comparison, SI-8, Figure S10b, presents the case where $E_{total} \approx E_{junction} + \Delta E_{Electrode}$ was the bias for topography imaging.

The simultaneously collected normalized current map (SI-7, Figure S9a) obtained during the chronoamperometric step, where the tip electrode potential was pulsed to -0.4 V for 20 ms, reveals heterogeneities that can be attributed to surface charge. A calibration curve of normalized current to surface charge density was calculated by the FEM model (SI-7, Figure S9b) from which Figure 5c was generated. It can be seen that the PC12 cell exhibited surface charge values of around -50 to -70 mC/m$^2$ with the glass having surface charge of around -20 to -40 mC/m$^2$, broadly in agreement with our previous measurements with conventional SICM,[8] that used the simplified model without EOF. The accuracy of the previous work could be improved by applying the new model herein, but the deductions would be similar.

**Reaction Mapping at a Carbon Fiber Electrode**

Although previous studies have considered using nanopipettes for molecular delivery,[17,24] there have been few attempts to quantify the effect of concentration gradients on electric potentials in SICM.[37] We now describe the use of ΔC-SICM to deliver reagent to a substrate electrode and map the resulting local electrochemical reaction *purely from the nanopipette response*. As

an exemplar system, we consider dopamine oxidation (unbuffered, pH 6.7) on a CF electrode (SI-4, Figure S4a for an optical micrograph of the substrate). CFs are widely used for studies of single neurons,[38] and other applications, but there is little information on the electrochemical response of these electrodes at the local level.

During the scan hopping CV regime implemented, the SICM bias between the two QRCEs was held constant at $E_{total} \approx \Delta E_{Electrode} + E_{junction} \approx 26\,\text{mV}$, a small positive value suitable for topographical imaging which also drives the migration of protonated dopamine ($Dop^+$),[38,39] out of the nanopipette, throughout the entire imaging process. Thus $Dop^+$ is pushed out the nanopipette by the applied bias but the *efflux rate* depends on the *local environment* (e.g. substrate reactions) and this is reflected in the *nanopipette current* (*vide infra*). During the approach of the nanopipette to the CF surface, the CF was held at a potential of -0.1 V vs. the Ag/AgCl QRCE in bulk so that no substrate electrode reaction occurred. When the nanopipette reached the near-surface (ca. 35 nm based on a set point of 3%), its position was fixed and the potential at the CF was swept from -0.1 V to 0.4 V and back again to -0.1 V in a CV at 1 V/s vs. the Ag/AgCl QRCE in bulk. The CF was then held at -0.1 V while the probe was retracted at a speed of 20 μm/s (retract distance 10 μm), and the same CV at the substrate was run with the probe now effectively in bulk solution. The tip ionic current response at the surface was normalized by that in bulk and is a measure of the relative conductance of the probe near the surface, with respect to the bulk during the substrate electrochemical reaction (see SI-4 for full details of the experimental setup and scanning regime).

An important consideration of these measurements is the spatial resolution of SICM for reaction mapping and delivery. This was explored using FEM simulations, with example results presented in Figure 6. For the conditions outlined above, Figure 6a shows a snapshot of the $Dop^+$ concentration around the pipette opening when the nanopipette was positioned 35 nm from the surface, before the reaction was driven. From this profile, we see that at these

separation distances, the high $Dop^+$ concentration is confined to the region directly beneath the pipette, suggesting the resolution of the technique is similar to the pipette dimensions. A profile of the $Dop^+$ concentration laterally along the substrate ($z$=0) is shown in Figure 6b for the cases where the nanopipette was at this approach distance (35 nm), and at the retract distance (~10 µm from the surface). It can be seen that the region of the substrate underneath the pipette has the greatest $Dop^+$ concentration and so this is where there would be the greatest change in ionic concentration owing to the substrate electrochemical reaction. By contrast, the profile with the tip at 10 µm from the substrate reveals a much smaller concentration of $Dop^+$ (max concentration of 0.01 mM) at the substrate surface and thus 10 µm can be reasonably considered to be bulk solution. These profiles of surface $Dop^+$ concentration are beneficial for determining the lateral hopping distance that should be used in ΔC-SICM delivery experiments in order to ensure that each pixel has not been exposed to significant amounts of dopamine from the prior approach that may lead to fouling of the substrate during oxidation.[40]

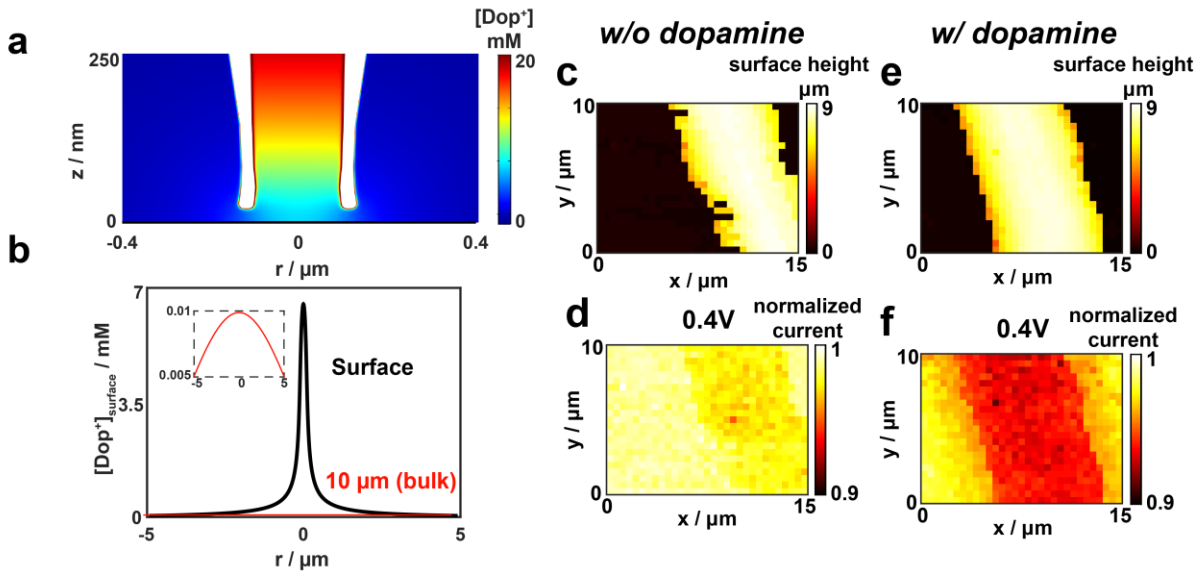


**Figure 6.** a) Simulated dopamine ($Dop^+$) concentration profile around the end of the nanopipette, positioned 35 nm away from a CF substrate. b) Near-surface concentrations of $Dop^+$ in the radial direction with the nanopipette 35 nm away from the surface (black line) and 10 µm away (red line), with the inset showing a zoom of data for the 10 µm distance case. Two

sets of example maps from electrode reaction mapping using ΔC-SICM with a nanopipette containing (c-d) 80 mM KCl (control case) and (e-f) 50 mM KCl and 30 mM dopamine hydrochloride (pH 6.7). (c,e) Topographical maps of two regions of the CF. (c,e) Individual frames taken from two videos of normalized nanopipette ionic current (in *x*,*y* as a function of substrate potential), at the substrate potential for dopamine oxidation (0.4 V: d,f). See SI-9, for the full movies.

This protocol was repeated at a series of pixels to create a spatial array of nanopipette current-substrate potential data sets that were used to make movies of normalized nanopipette current in *x*-*y* space as a function of applied substrate potential. These map the progress of the substrate reaction both spatially and with potential resolution. Scans were taken: with the probe containing only 80 mM KCl (control case); and 50 mM KCl and 30 mM dopamine hydrochloride. In both cases, the bulk solution contained 10 mM KCl (more dilute than the tip). Full videos of the voltammetric response in each case are shown in SI-9, SI_Control.avi and SI_Dopamine.avi.

Snapshots from the 2 movies at the most extreme (diffusion-limited) potential of +0.4 V *vs*. Ag/AgCl QRE are shown in Figure 6, together with the topographical maps obtained simultaneously. The topographical maps (Figure 6c,e) are closely similar, clearly resolving the 7 μm diameter CF. When a potential of +0.4 V was applied to the CF, dopamine oxidation occurred at a diffusion-controlled rate (bulk voltammetry shown in SI-4, Figure S5), and there is a clear difference between the scan in which dopamine is absent (Figure 6d) and the scan in which it is present in the nanopipette (Figure 6f). With dopamine present, the ionic current drops by a consistent 7-8% at each pixel across the surface of the CF. This is because the substrate acts as a sink for $Dop^+$.[40] Whilst protons are released in $Dop^+$ electrooxidation,[29] which should enhance the conductivity of the gap, the majority of the resistance in SICM

experiments comes from the nanopipette itself, and $Dop^+$ consumption at the CF depletes the concentration in the end part of the tip, while substrate-generated protons are excluded by the direction of the applied electric field at the tip. The result is an increase in resistance and hence decrease in the overall ionic current. This change in ionic current is also seen at the pixels surrounding the CF, a "diffusional broadening", caused by the sink-like nature of the CF. A small decrease in the ionic current (1-2%) can also be seen over the surface of the CF for the control (Figure 6d), suggesting that a small current is driven between the CF electrode and the QRCE in the probe. This is an interesting observation that might have future applications, but the effect is far less than with dopamine present (Figure 6f).

The movie SI_Dopamine.avi shows that there is considerable heterogeneity in the spatial current (substrate reactivity) for $Dop^+$ delivery, in the region of the CF, at potentials less than the diffusion-limit, indicating spatial variation in reaction rate. In the future, coupling such movies with data from other microscopy techniques in a multimicroscopy approach, as we have advocated elsewhere for other electrochemical probe techniques,[9,10] could be particularly illuminating of surface reactivity.

## CONCLUSIONS

In this paper we have provided a full analysis of the electrochemical potentials and mass transport in SICM, particularly pertinent to the case where different concentrations, or solution compositions, are employed in the nanopipette and bulk solutions, but also of value for conventional SICM. Through this analysis, we have demonstrated the versatility and advantages of using different ionic strength media in the SICM tip and bulk solution, in a mode termed ΔC-SICM. Notably, topographical imaging with much reduced electric field than in conventional (applied bias SICM) becomes possible by driving the ionic current purely through the junction (diffusion) potential, due to the concentration gradient at the end of the

nanopipette. Functional applications, such as charge mapping with ΔC-SICM, are more sensitive than conventional SICM, with the charge sensitivity arising from significant EOF effects in this configuration. The model developed, which solves the Poisson, Nernst-Planck and Navier-Stokes equations with EOF, can also be applied to conventional SICM charge mapping measurements and allows for a more accurate determination of high surface charge densities than our previous approach.

This work has expanded on the use of SICM for the delivery of charged molecules to a surface. One can envisage many applications, spanning cell biology, electrochemistry and catalysis, where a nanopipette could be used for delivery and to measure spatial variations in efflux rate simply through the nanopipette current.

## SUPPORTING INFORMATION

Supporting Information includes: determined QRCE potentials in different media, example topographical maps with ΔC-SICM, details of the surface charge mapping protocol and FEM simulations, raw data corresponding to Figure 4, further surface charge mapping data and a schematic and optical data of the carbon fiber device and a full image sequence (movies) of the voltammetric data presented in Figure 6.

## CONFLICT OF INTEREST

The authors declare no competing financial interest.

## ACKNOWLEDGEMENTS

DP was supported through a Leverhulme Trust Research Project Grant. AP was supported by the EPSRC through the MOAC DTC, grant number EP/F500378/1. BC acknowledges support from the Warwick-China Scholarship Council for a joint scholarship. PRU acknowledges

support from a Royal Society Wolfson Research Merit Award. We thank Dr. Joanna Collingwood for the use of the cell culturing facility, Dr. Phillip Young for cell culturing training, Mareike Herrmann for help constructing the CF samples and Dr. Martin Edwards (University of Utah) for advice with FEM simulations.

**REFERENCES**

(1) Hansma, P. K.; Drake, B.; Marti, O.; Gould, S. A.; Prater, C. B. *Science.* **1989**, 243, 641–643.

(2) Chen, C.-C.; Zhou, Y.; Baker, L. A. *Annu. Rev. Anal. Chem.* **2012**, 5, 207–228.

(3) Korchev, Y. E.; Bashford, C. L.; Milovanovic, M.; Vodyanoy, I.; Lab, M. J. *Biophys. J.* **1997**, 73, 653–658.

(4) Korchev, Y. E.; Milovanovic, M.; Bashford, C. L.; Bennett, D. C.; Sviderskaya, E. V; Vodyanoy, I.; Lab, M. J. *J. Microsc.* **1997**, 188, 17–23.

(5) Novak, P.; Li, C.; Shevchuk, A. I.; Stepanyan, R.; Caldwell, M.; Hughes, S.; Smart, T. G.; Gorelik, J.; Ostanin, V. P.; Lab, M. J.; Moss, G. W. J.; Frolenkov, G. I.; Klenerman, D.; Korchev, Y. E. *Nat Meth* **2009**, 6, 279–281.

(6) Gorelik, J.; Zhang, Y.; Shevchuk, A. I.; Frolenkov, G. I.; Sánchez, D.; Lab, M. J.; Vodyanoy, I.; Edwards, C. R. W.; Klenerman, D.; Korchev, Y. E. *Mol. Cell. Endocrinol.* **2004**, 217, 101–108.

(7) Perry, D.; Paulose Nadappuram, B.; Momotenko, D.; Voyias, P. D.; Page, A.; Tripathi, G.; Frenguelli, B. G.; Unwin, P. R. *J. Am. Chem. Soc.* **2016**, 138, 3152–3160.

(8) Page, A.; Perry, D.; Young, P.; Mitchell, D.; Frenguelli, B. G.; Unwin, P. R. *Anal. Chem.* **2016**, 88, 10854–10859.

(9) Kang, M.; Momotenko, D.; Page, A.; Perry, D.; Unwin, P. R. *Langmuir* **2016**, 32, 7993–8008.

(10) Page, A.; Perry, D.; Unwin, P. R. *Proc. R. Soc. A Math. Phys. Eng. Sci.* **2017**, 473, 20160889.

(11) Chen, C.-C.; Baker, L. A. *Analyst* **2011**, 136, 90–97.

(12) McKelvey, K.; Perry, D.; Byers, J. C.; Colburn, A. W.; Unwin, P. R. *Anal. Chem.* **2014**, 86, 3639–3646.

(13) Li, P.; Liu, L.; Yang, Y.; Zhou, L.; Wang, D.; Wang, Y.; Li, G. *J. Lab. Autom.* **2015**, 20, 457–462.

(14) Takahashi, Y.; Murakami, Y.; Nagamine, K.; Shiku, H.; Aoyagi, S.; Yasukawa, T.; Kanzaki, M.; Matsue, T. *Phys. Chem. Chem. Phys.* **2010**, 12, 10012–10017.

(15) Yang, X.; Liu, X.; Zhang, X.; Lu, H.; Zhang, J.; Zhang, Y. *Ultramicroscopy* **2011**, 111, 1417–1422.

(16) Momotenko, D.; McKelvey, K.; Kang, M.; Meloni, G. N.; Unwin, P. R. *Anal. Chem.* **2016**, 88, 2838–2846.

(17) Perry, D.; Al Botros, R.; Momotenko, D.; Kinnear, S. L.; Unwin, P. R. *ACS Nano* **2015**, 9, 7266–7276.

(18) Klausen, L. H.; Fuhs, T.; Dong, M. *Nat. Commun.* **2016**, 7, 12447.

(19) Page, A.; Kang, M.; Armitstead, A.; Perry, D.; Unwin, P. R. *Anal. Chem.* **2017**, 89, 3021–3028.

(20) McKelvey, K.; Kinnear, S. L.; Perry, D.; Momotenko, D.; Unwin, P. R. *J. Am. Chem. Soc.* **2014**, 136, 13735–13744.

(21) Schobesberger, S.; Jönsson, P.; Buzuk, A.; Korchev, Y.; Siggers, J.; Gorelik, J. *Biophys. J.* **2016**, 110, 141–146.

(22) Momotenko, D.; Page, A.; Adobes-Vidal, M.; Unwin, P. R. *ACS Nano* **2016**, 10, 8871–8878.

(23) Bruckbauer, A.; Ying, L.; Rothery, A. M.; Zhou, D.; Shevchuk, A. I.; Abell, C.;

Korchev, Y. E.; Klenerman, D. *J. Am. Chem. Soc.* **2002**, 124, 8810–8811.

(24) Rodolfa, K. T.; Bruckbauer, A.; Zhou, D.; Korchev, Y. E.; Klenerman, D. *Angew. Chemie - Int. Ed.* **2005**, 44, 6854–6859.

(25) Ying, L.; Bruckbauer, A.; Rothery, A. M.; Korchev, Y. E.; Klenerman, D. *Anal. Chem.* **2002**, 74, 1380–1385.

(26) Edwards, M. A.; Williams, C. G.; Whitworth, A. L.; Unwin, P. R. *Anal. Chem.* **2009**, 81, 4482–4492.

(27) Takahashi, Y.; Ito, K.; Wang, X.; Matsumae, Y.; Komaki, H.; Kumatani, A.; Ino, K.; Shiku, H.; Matsue, T. *Electrochemistry* **2014**, 82, 331–334.

(28) Perry, D.; Momotenko, D.; Lazenby, R. A.; Kang, M.; Unwin, P. R. *Anal. Chem.* **2016**, 88, 5523–5530.

(29) Al-Sakere, B.; André, F.; Bernat, C.; Connault, E.; Opolon, P.; Davalos, R. V; Rubinsky, B.; Mir, L. M. *PLoS One* **2007**, 2, e1135.

(30) Davalos, R. V; Mir, L. M.; Rubinsky, B. *Ann. Biomed. Eng.* **2005**, 33, 223–231.

(31) Miklavčič, D.; Beravs, K.; Šemrov, D.; Čemažar, M.; Demšar, F.; Serša, G. *Biophys. J.* **1998**, 74, 2152–2158.

(32) Bard, A. J.; Faulkner, L. R.; Leddy, J.; Zoski, C. G. *Electrochemical methods: fundamentals and applications*; Wiley New York, 1980; Vol. 2.

(33) White, H. S.; Bund, A. *Langmuir* **2008**, 24, 2212–2218.

(34) Momotenko, D.; Cortes-Salazar, F.; Josserand, J.; Liu, S.; Shao, Y.; Girault, H. H. *Phys. Chem. Chem. Phys.* **2011**, 13, 5430–5440.

(35) Babakinejad, B.; Jönsson, P.; López Córdoba, A.; Actis, P.; Novak, P.; Takahashi, Y.; Shevchuk, A.; Anand, U.; Anand, P.; Drews, A.; Ferrer-Montiel, A.; Klenerman, D.; Korchev, Y. E. *Anal. Chem.* **2013**, 85, 9333–9342.

(36) Bath, B. D.; Michael, D. J.; Trafton, B. J.; Joseph, J. D.; Runnels, P. L.; Wightman, R.

M. *Anal. Chem.* **2000**, 72, 5994–6002.

(37) Patel, A. N.; Tan, S. Y.; Miller, T. S.; Macpherson, J. V.; Unwin, P. R. *Anal. Chem.* **2013**, 85, 11755–11764.

(38) Patel, A. N.; McKelvey, K.; Unwin, P. R. *J. Am. Chem. Soc.* **2012**, 134, 20246–20249.

**for TOC only**

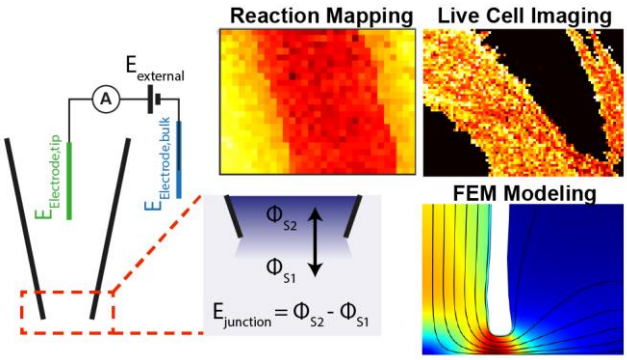
Reaction Mapping
Live Cell Imaging
E external
A
E Electrode,tip
E Electrode,bulk
Φ S2
Φ S1
E junction = Φ S2 - Φ S1
FEM Modeling